Mon. Not. R. Astron. Soc. **000**, 000–000 (0000) Printed 1 February 2008 (MN LATEX style file v1.4)

ASCA PV observations of the Seyfert 2 galaxy NGC 4388: the obscured nucleus and its X-ray emission

K. Iwasawa[1], A.C. Fabian[1], S. Ueno[2], H. Awaki[2], Y. Fukazawa[3], K. Matsushita[3] and K. Makishima[3]

1: Institute of Astronomy, Madingley Road, Cambridge CB3 0HA
2: Department of Physics, Kyoto University, Sakyo-ku, Kyoto 606-01, Japan
3: Department of Physics, the University of Tokyo, Hongo, Bunkyo-ku, Tokyo 113, Japan

ABSTRACT

We present results on the Seyfert 2 galaxy NGC4388 in the Virgo cluster observed with *ASCA* during its performance verification (PV) phase. The 0.5–10 keV X-ray spectrum consists of multiple components; (1) a continuum component heavily absorbed by a column density $N_{\rm H} \approx 4 \times 10^{23}{\rm cm}^{-2}$ above 3 keV; (2) a strong 6.4 keV line (equivalent width $EW \sim 500$ eV); (3) a weak flat continuum between 1 and 3 keV; and (4) excess soft X-ray emission below 1 keV. The detection of strong absorption for the hard X-ray component is firm evidence for an obscured active nucleus in this Seyfert 2 galaxy. The absorption corrected X-ray luminosity is about 2×10^{42}erg s^{-1}. This is the first time that the fluorescent iron-K line has been detected in this object; the large EW is a common property of classical Seyfert 2 nuclei. The flat spectrum in the intermediate energy range may be a scattered continuum from the central source. The soft X-ray emission below 1 keV can be thermal emission from a temperature $kT \simeq 0.5$ keV, consistent with the spatially extended emission observed by *ROSAT* HRI. However, the low abundance ($Z \sim 0.05 Z_{\odot}$) and high mass flow rate required for the thermal model and an iron-K line stronger than expected from the obscuring torus model are puzzling. An alternative consistent solution can be obtained if the central source was a hundred times more luminous over than a thousand years ago. All the X-ray emission below 3 keV is then scattered radiation.

Key words:

1 INTRODUCTION

NGC4388 is an active galaxy situated near the core of the Virgo cluster. The spiral stellar disk (SB(s)b pec; Phillips & Malin 1982) is viewed nearly edge-on (inclination $\sim 72^{\circ}$) with a dust lane across near the nucleus. The distance of the galaxy is assumed to be 19.7 Mpc (Sandage & Tammann 1984) throughout this paper, giving an angular scale of 95.5 pc arcsec^{-1}. The blue and far infrared luminosities are $L_{\rm B} \simeq 6.4 \times 10^{43}$erg s^{-1} and $L_{\rm FIR} \simeq 2.7 \times 10^{43}$erg s^{-1}, assuming this distance (David, Jones & Forman 1992).

Optical spectra of the nucleus show emission lines characteristic of a Seyfert type 2 galaxy (Phillips & Malin 1982; Phillips, Charles & Baldwin 1983). An anisotropic ionization field is indicated by the cones of highly-ionized line emission extending above and below the stellar disk (Colina et al 1987; Pogge 1988). Gas emitting [OIII]λ5007 extends as far as 50 arcsec ($\sim$5kpc) from the nucleus (Pogge 1988). The ionization state of the gas is best described as due to photoionization by a powerful nonthermal source (Pogge 1988; Colina 1992). Collimation of the nuclear radiation is strongly supported by the VLA images (Stone, Wilson & Ward 1988; Hummel & Saikia 1991).

The detection of a weak broad wing to Hα (FWZI $\simeq$ 6000 km s^{-1}) reported by Filippenko & Sargent (1985) suggests the presence of a Seyfert 1 nucleus obscured from our direct view. Shields & Filippenko (1988, 1996) also find off-nuclear broad Hα emission (FWZI $\simeq$4000 km s^{-1}) arising within the biconical high-ionization regions observed by Pogge (1988). A plausible origin for these properties is the scattering of line emission from a hidden Broad Line Region.

A strong hard X-ray source in NGC4388 has been detected by the Birmingham X-ray coded mask telescope (SL2 XRT: Hanson et al 1990), the *Ginga* LAC (Takano & Koyama 1991) and SIGMA (Lebrun et al 1992), supporting the hypothesis of a powerful hidden nucleus. The results suggest the presence of a power-law X-ray source of photon index, $\Gamma \approx 1.5$, absorbed by a column density $N_{\rm H} \sim$ a few times $10^{23}{\rm cm}^{-2}$. The absorption-corrected, 2–10 keV lumi-

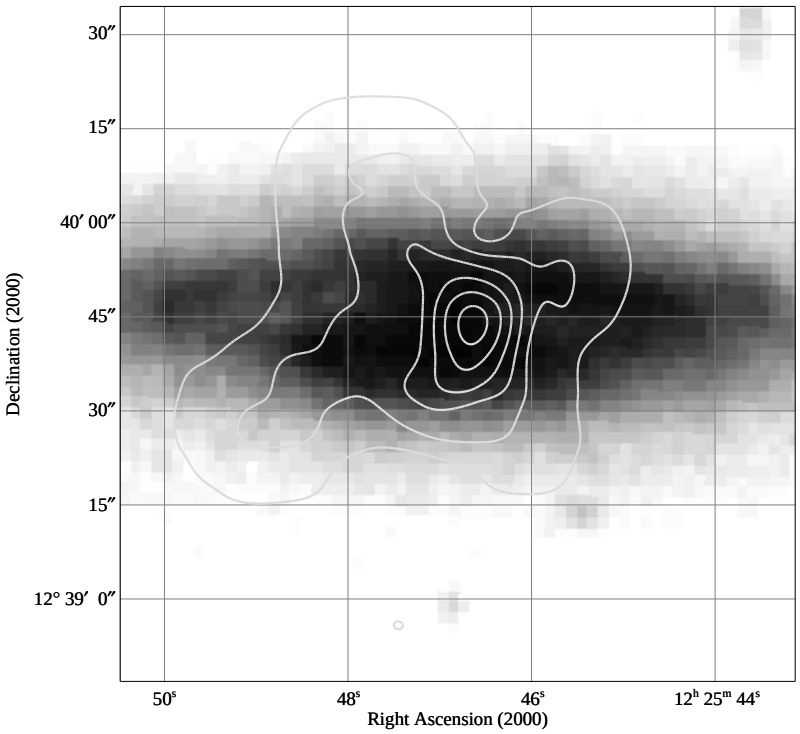

Figure 1. The *ROSAT* HRI image (Matt et al 1994) overlaid on the blue optical band image taken from the Palomer 48-inch Schmidt Digitized Sky Survey.

nosity $L_{\rm X}$=2×10^{42} erg s^{-1}, is typical for a low luminosity Seyfert 1 galaxy.

The origin of weak soft X-ray emission seen from the source is, on the other hand, controversial The soft X-ray luminosity, $L_{0.5-3{\rm keV}} = 1.5 \times 10^{40}$erg s^{-1}, first detected by the *Einstein Observatory* (Forman et al 1979), is $\sim$1 per cent of the absorption-corrected luminosity of the hard X-ray source and consistent with the possibility that the soft X-rays are scattered nuclear radiation. However, the *ROSAT* HRI image of NGC4388 shows the 0.1–2.4 keV emission to be clearly extended with a radius of 45 arcsec and luminosity $L_{\rm X} \simeq 3 \times 10^{40}$erg s^{-1}(Matt et al 1994; see also Fig. 1). The radial profile shows that half of the soft X-ray emission originate beyond the central 15 arcsec. Matt et al (1994) claim that the large extent is evidence against a scattering origin for the soft X-ray emission, since the X-ray luminosity of the central source implied by the hard X-ray observations is insufficient to photoionize the necessary column density. They propose as alternative explanations either thermal emission from a starburst or a collection of discrete sources. The *ROSAT* PSPC spectrum shows a steep spectral slope, Γ =2–3 (Rush & Malkan 1996) which may be consistent with this interpretation. However, the spectral resolution of these instruments does not provide any conclusive evidence.

We report here the first *ASCA* results on NGC4388 (see Tanaka, Inoue & Holt 1994 for a brief discussion of the capabilities of *ASCA*). The superior spectral resolution of *ASCA* over the 0.5–10 keV band enables us to identify several different components in the spectrum.

2 THE ASCA OBSERVATIONS AND DATA REDUCTION

2.1 Observations

NGC4388 was observed in two different pointings at adjacent elliptical galaxies in the Virgo cluster, M86 (NGC4406; *ASCA* results of this galaxy appear in Awaki et al 1994 and Matsushita et al 1994) and M84 (NGC4374) during the *ASCA* performance verification (PV) phase. These observations were carried out in series between 1993 July 3 and 4, each with an effective exposure time of about 20 ks. NGC4388 was off axis by 18 and 10 arcmin, respectively. In the first observation, NGC4388 was outside the field of view of the Solid state Imaging spectrometer (SIS) detector so no SIS data was obtained. Data reduction was made using the *ASCA* standard softwares, XSELECT and FTOOLS. One dataset of effective exposure time 17 ks for both SIS (S0 and S1), and two datasets of each 20 ks were obtained for both Gas Imaging Spectrometers (GIS: G2 and G3).

2.2 The image

The full band (0.7–10 keV) GIS image from the first observation is shown in Fig. 2. The two elliptical galaxies, M86 and M84 are present in the field of view as well as NGC4388. Distortion of the X-ray image of NGC4388 is due to the off-axis response of the X-ray Telescope (XRT) and is consistent with the point spread function at that position (the elongation of the image aligning with the galaxy major axis is a coincidence). The SIS image obtained at a small off-axis po-

sition does not show evidence for significant extended emission within the spatial resolution of ASCA. Fig. 3 indicates that NGC4388 is the only strong source in the energy band above 3 keV but is faint in the softer band. Significant X-ray emission at the position of NGC4388 is, however, detected both in the GIS and SIS in the energy band below 3 keV as an excess above the diffuse emission spreading out from the M86 direction.

2.3 Spectral data and diffuse background

Energy spectra were extracted from an elliptical-shaped region with the major axis aligned with the elongation of the image (3×1.6 arcmin for the SIS; 5×3 arcmin for the GIS).

Background subtraction must be done carefully, both because of the weakness of NGC4388 itself and the complex underlying diffuse emission in this busy field. Since NGC4388 lies close to the core of the Virgo cluster there is significant emission from the intra-cluster medium (ICM). The temperature of the ICM, $kT \approx 2.5$ keV, has been measured with *Ginga* (Koyama, Takano & Tawara 1991) and *ROSAT* (Böhringer et al 1994). In addition, there may be some extended emission from M86* which makes the background around NGC4388 complicated.

We have checked the background data by dividing it into four distinct regions. The data taken from the far side (SW of NGC4388) of M86 and M84 are weaker than in the other directions and show a different spectral shape. This implies that the diffuse emission has a gradient in intensity and spectrum across the source-extracted region of NGC4388. We thus took background data from a circular, annulus of width 5 arcmin for the SIS and a circular or an elliptical annulus (depending on off-axis angle) with a radius of 6–8 arcmin for the GIS. The background used here should be a good approximation of the true background, since taking data from the region surrounding the source should smear the gradient out.

The background-subtracted count rate in each detector is shown in Table 1. The source fraction of the total counts in the source-extraction region for each detector is about 70 per cent for the SIS data, 60 per cent for the first GIS data, and 68 per cent for the second GIS data. We find no obvious change in observed flux during each observation. Any possible flux change is less than ±30 per cent during each $\sim$ 40 ks long observation (net exposure time is $\sim$20 ks in each). Differences of count rate between the two GIS observations (Table 1) are owing to differences of effective area of the photon collecting region at the given off-axis positions. The effective area obtained through the XRT and GIS responses in the first observation is $\sim$ 48 per cent of that in the second observation. This means that there is no significant change in source flux between the two observations after the correction.

3 RESULTS

* Awaki et al (1994) give a temperature of $kT = 0.79 \pm 0.01$ keV and abundance $Z = 0.45^{+0.13}_{-0.08} Z_\odot$ for the total X-ray emission of M86 after fitting with a Raymond-Smith thermal spectrum model.

Observation	S0	S1	G2	G3
1st [ct s^{-1}]	—	—	0.028	0.020
2nd [ct s^{-1}]	0.050	0.038	0.055	0.048

Table 1. The background-subtracted count rate in each detector. There is no SIS data in the first observation. NGC4388 is observed at off-axis angle $\sim$ 18 arcmin in the first observation, and $\sim$ 10 arcmin in the second observation. The effective area of the source-photon collected region of NGC4388 in the first observation is $\sim$ 48 per cent of that in the second observation.

3.1 Spectral fitting

We have two SIS and four GIS spectra. Since the off-axis position of the source (and thus the effective area of the XRT) is different for the first and second observations, we treat the two GIS data sets separately, and fit the four spectra jointly. There is some difference in the soft X-ray emission detected by the SIS and GIS data. This is probably due to uncertainties in background subtraction; we include it as a systematic uncertainty in our subsequent analysis. Since we believe the background subtraction is not seriously incorrect, from the detailed inspection discussed in Section 2.3, errors due to background subtraction in the individual detectors should be smaller than the systematic uncertainty, even in the soft X-ray band.

3.1.1 The Hard X-ray components

As Fig. 4 and Fig. 5 show, a strong continuum excess is seen above 3 keV with a sharp emission line around 6.4 keV. This feature is identified as the K-shell fluorescence line from cold iron. The hard X-ray spectrum is well fitted by an absorbed power-law and a gaussian line. The photon-index and absorption column density depend on the precise spectral model chosen for the soft X-ray component (see later).

3.1.2 A Spectral model for the soft X-ray components

We first examined the SIS data below 3 keV, since the spectral resolution and detection efficiency for soft X-rays are better in the SIS than the GIS. A simple power-law does not give a good fit ($\chi^2 = 74.38$ for 41 degrees of freedom). The best-fit photon index is $\Gamma = 1.6 \pm 0.4$ with the Galactic absorption $N_{\rm H} = 3 \times 10^{20} {\rm cm}^{-2}$, which is consistent with the *ROSAT* PSPC result, $\Gamma \sim$2–3 (Rush & Malkan 1996). There is a significant line-like excess around 0.8 keV, which could be due to an iron L-shell emission bump. Since the soft X-ray emission of NGC4388 is spatially extended, as observed by the *ROSAT* HRI (Matt et al 1994), this feature is probably due to the thermal emission from ionized gas associated with the galaxy. However, a thermal spectrum of a temperature implied from the 0.8 keV peak ($kT \sim 0.5$ keV) alone cannot explain all the emission below 3 keV. A power-law fit to the 1–3 keV data indicates that the spectrum is flat, with $\Gamma = 1.0 \pm 0.4$, and inconsistent with the thermal spectrum characterized by the 0.8 keV peak, which is much steeper in this energy band. Another component is required to explain the flat spectrum. If this is another thermal emission component in the galaxy, a temperature would be much larger than 10 keV.

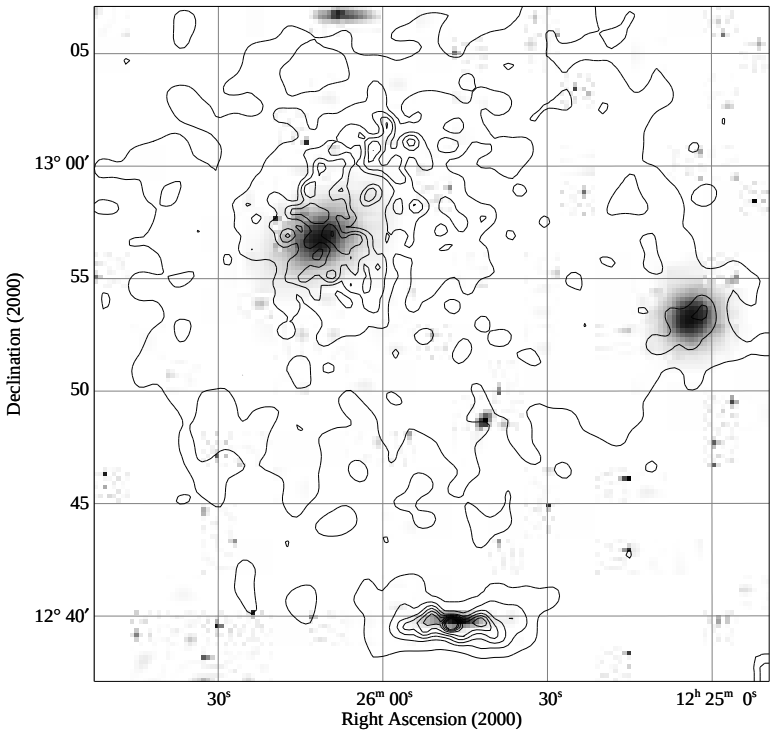

Figure 2. Full-band (0.7–10 keV) GIS image from the first observation, overlaid on the digital sky survey image in the optical band. X-ray emission was detected from three galaxies in the field of view; M86 (middle), M84 (right), and NGC4388 (below).

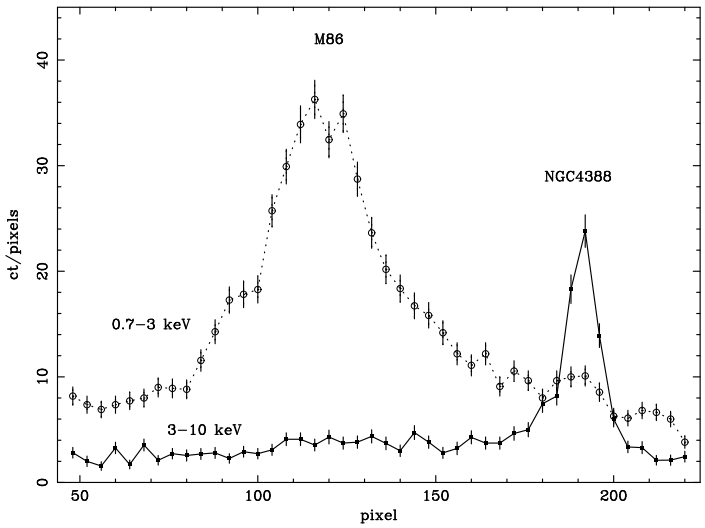

Figure 3. Projected images across M86 and NGC4388 in two energy bands; open circles with a dotted line: 0.7–3 keV; and filled squares with a solid line: 3–10 keV. 1 pixel corresponds to 0.25 arcmin.

Possible origins for the flat spectrum are; a) scattered nuclear continuum, b) part of the transmitted nuclear continuum, and c) a collection of high-mass X-ray binaries. These will be discussed in Section 4. In subsequent fits, the component is modelled by a power-law.

Thus a thermal spectrum plus a power-law can be an appropriate model for the soft X-ray spectrum. We use a Raymond-Smith thermal spectrum assuming only Galactic absorption, since this extended component may be free from

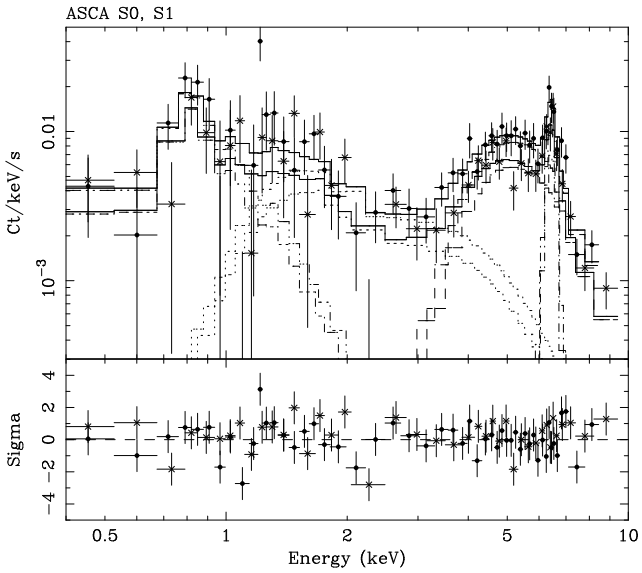

Figure 4. The *ASCA* SIS spectra of NGC4388. Filled circles are the S0 data and crosses are the S1 data. The best-fit model in Table 2 is shown in the stepped-lines. Spectral components are also shown.

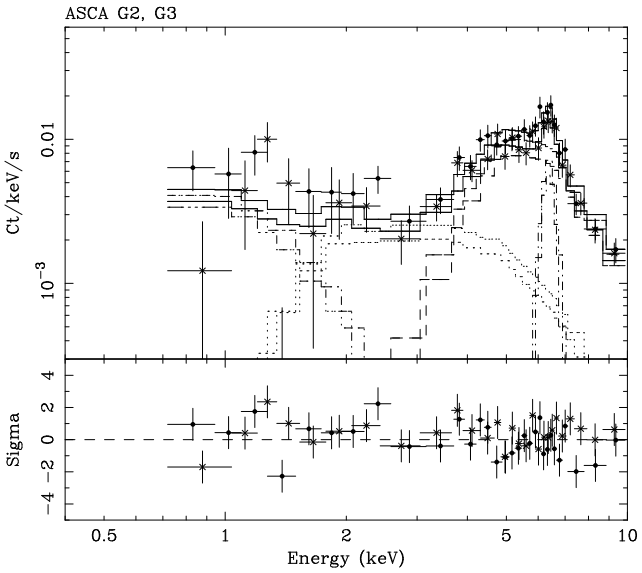

Figure 5. The *ASCA* GIS spectra of NGC4388. The data from the second observation only are shown for clarity. Filled circles are G2 data and crosses are G3 data. The best-fit model and spectral components in Table 2 are also shown.

the intrinsic absorption of the host galaxy. The absorption for the power-law component remains a free parameter.

3.1.3 The spectrum of the whole energy band

The whole spectrum is fitted using the above two soft X-ray components in addition to the absorbed power-law plus a gaussian. The photon-index of the soft power-law component (PL_2) is not well constrained. Thus it is assumed to be identical to the hard power-law (PL_1). The GIS is less sensitive to the thermal component because of its poorer spectral resolution and limited efficiency below 1 keV. Constraints on the temperature and abundance are worse than those from the SIS data. The parameters of the thermal component are therefore fixed at the SIS-derived values, except for the normalization, when fitting the GIS spectra. The results are shown in Table 2, and the best-fit models for the both detectors are shown in Fig. 4 and Fig. 5, respectively.

We detected strong absorption $N_{\rm H} \approx 4 \times 10^{23}{\rm cm}^{-2}$ for the hard X-ray component, with a relatively small uncertainty compared with previous measurement (see Table 2). The constraint on the photon index is weak owing to the limited energy range and strong absorption. The best-fit $\Gamma \approx 1.6$ is consistent with previous results (Hanson et al 1990; Takano & Koyama 1991). A strong fluorescence iron Kα line is found for the first time in this object. The equivalent width (EW) is quite large despite the relatively narrow line width. There is no evidence for the line broadening in the GIS data whereas there is weak evidence ($\sigma = 0.14^{+0.13}_{-0.06}$ keV) in the SIS data. When we assume that the PL_2 has an identical Γ to the PL_1, some extra absorption, $N_{\rm H} \approx (1-3) \times 10^{22}$ cm^{-2}, is required (see Table 2). This means that the soft X-ray spectrum around 2 keV is extremely flat.

3.1.4 X-ray fluxes

The observed fluxes are summarized in Table 3. The flux in the 3–10 keV band is slightly smaller than that observed by the SL2 XRT ($f_{3-10{\rm keV}} = 2.0 \times 10^{-11}$erg cm^{-2} s^{-1}; Hanson et al 1990). The soft X-ray flux is roughly consistent with previous measurements from the *ROSAT* PSPC ($f_{0.1-2{\rm keV}} = 4.7 \times 10^{-13}$erg cm^{-2} s^{-1}, Rush & Malkan 1996) and the *ROSAT* HRI ($f_{0.1-2.4{\rm keV}} = 5.8 \times 10^{-13}$erg cm^{-2} s^{-1}, Matt et al 1994), extrapolating our best-fit model down to 0.1 keV, although the *ROSAT* flux depends on the assumed model.

4 DISCUSSION

4.1 The obscured nucleus

We find clear evidence for strong obscuration along the line of sight. The column density $N_{\rm H} \approx 4 \times 10^{23}{\rm cm}^{-2}$ implied from the *ASCA* spectrum is similar to those observed in some other classical Seyfert 2 galaxies (e.g., Awaki et al 1991; Iwasawa et al 1994). The photon index ($\Gamma \approx 1.6$) is also consistent with that of Seyfert galaxies. Our best-fit value can be justified by the fact that a *SIGMA* observation in the 40–150 keV band (Lebrun et al 1992) is in agreement with an extrapolation of the result of Hanson et al (1990), unless any extra component, e.g. Compton reflection component, has a significant contribution at the hard X-ray band (the

	PL_1		Fe K line			PL_2		R-S		N_2/N_1	χ^2/dof
	Γ_1	N_{H1} 10^{23}cm^{-2}	E keV	σ keV	EW eV	Γ_2	N_{H2} 10^{22}cm^{-2}	kT keV	$Z/Z_\odot$		
SIS	$1.6^{+0.5}_{-0.4}$	$4.2^{+0.6}_{-1.0}$	$6.44^{+0.05}_{-0.05}$	$0.14^{+0.13}_{-0.06}$	732^{+243}_{-191}	$=\Gamma_1$	$1.1^{+0.8}_{-0.9}$	$0.47^{+0.18}_{-0.17}$	$0.053^{+0.35}_{-0.03}$	0.030	93.84/81
GIS	$1.5^{+0.4}_{-0.5}$	$3.7^{+1.0}_{-0.5}$	$6.39^{+0.06}_{-0.07}$	$0.06^{+0.17}_{-0.06}$	438^{+127}_{-102}	$=\Gamma_1$	$3.1^{+2.1}_{-1.9}$	0.47	0.053	0.055	219.8/220

Table 2. Spectral fits to *ASCA* data of NGC4388. The best-fit parameters are shown for the SIS and the GIS datasets. The first and second data sets for the GIS were fitted jointly. 'PL_1' and 'PL_2' stand for a power-law for the hard and soft components, respectively, and 'R-S' for the Raymond-Smith thermal spectrum. 'N_2/N_1' is a normalization ratio of the PL_2 and PL_1. These best-fit models are indicated in Fig. 4 and Fig. 5.

f_X	SIS	GIS
0.5–10 keV [$\times 10^{-11}$erg cm^{-2} s^{-1}]		
Total	1.6	1.4
0.5–3 keV [$\times 10^{-13}$erg cm^{-2} s^{-1}]		
Total	6.4	6.5
R-S	2.9	4.4
PL_2	3.5	2.1
3–10 keV [$\times 10^{-11}$erg cm^{-2} s^{-1}]		
Total	1.6	1.4
PL_1	1.3	1.1
PL_2	0.11	0.15

Table 3. Observed X-ray fluxes in various energy bands. Flux of each spectral component is also shown, which is derived from the best-fit model in Table 2. Note that the total flux in the 3–10 keV band include the iron K line flux.

reflection contribution should be small if the inner disk is highly inclined to our line of sight).

The absorption-corrected 2–10 keV flux of the hard power-law component is $(4.3 \pm 0.6) \times 10^{-11}$erg cm^{-2} s^{-1}, corresponding to a luminosity, $L_{2-10\mathrm{keV}} = (1.9 \pm 0.3) \times 10^{42}$erg s^{-1}. This is within the range of Seyfert 1 nuclei. Colina (1992) predicted that a UV luminosity, $L_{\mathrm{UV}} = 1.7 \times 10^{43}$erg s^{-1}, is required to explain the high ionization extended nebula. If NGC4388 has the ratio, $L_X/L_{\mathrm{UV}} \sim 0.1$, generally appropriate for active galaxies, then the intrinsic X-ray luminosity of the central source is reasonable. This agreement may imply that the radiation of the central continuum is not significantly anisotropic, because the X-ray measurement is for line-of-sight radiation while the calculation of the UV luminosity is made for the ionized nebulae extending perpendicular to the line-of-sight.

The implied heavy obscuration is opaque to the optical/UV continuum from the central source, unless the dust to gas ratio is unusually low. Even in the near-infrared band, HeIλ1.083μm and Pa$\beta\lambda$1.28μm do not show any broad component (Ruiz, Rieke & Schmidt 1994). The displacement between the optical nucleus and the radio/10μm peak (Stone et al 1988) is likely due to this obscuration effect, and the true nucleus should be at the radio/10μm nucleus position. Even though deficits of HI and CO gas in this galaxy have been reported (Chamaraux, Balkowski, & Gerard 1980; Kenney & Young 1986), plenty of cold gas remains close to the central X-ray source. This can form an obscuring torus such as proposed in the unification scheme of Seyfert galaxies (e.g., Antonucci 1993). The anisotropic radio source extending perpendicular to the galaxy (Stone et al 1988; Hummel & Saikia 1991) and the conical high-ionization regions observed in the optical band (Pogge 1988; Colina et al 1987) are compatible with the idea of collimation of radiation by the torus. We note that the symmetrical axes of the torus and the stellar disk of NGC4388 are aligned as well as NGC4945 (Iwasawa et al 1993), while they are misaligned in most cases (e.g., NGC1068, Antonucci & Miller 1985; NGC5252, Tadhunter & Tsvetanov 1989).

An alternative source of the strong X-ray absorption is the interstellar medium in the nearly edge-on galaxy disk itself. Recent near-infrared imaging has revealed that this galaxy has a boxy bulge (McLeod & Rieke 1995). This and the dust lane crossing in front of the nucleus can be responsible for some or all of the absorption. In this case, the flat spectrum between 1 and 3 keV is possibly explained by transmission of scattered radiation from the central source seen through the stellar disk. Since the disk is tilted by $\sim$ 18 degrees from being exactly edge-on, there may be less absorption along these lines of sight, so making a flat spectrum in the softer band in addition to the strongly absorbed component.

We note there will be some scattering in the obscuring medium with $N_{\mathrm{H}} \sim 4 \times 10^{23}$cm^{-2} leading to a hard power-law component in the 1–3 keV band (Yaqoob 1996). This, however, is at least an order of magnitude fainter than the observed power-law in that band, unless the absorbing medium is partially ionized.

4.2 The iron K line

A strong iron Kα emission line is detected at 6.4 keV. The large equivalent width ($EW = 440 - 730$ eV) of the 6.4 keV line is one of the signatures of reprocessing in cold matter. Various calculations of X-ray spectra emerging from a central power-law source surrounded by a torus do predict a large EW (Awaki et al 1991; Krolik, Madau & Życki 1994; Ghisellini, Haardt & Matt 1994). However, the observed EW is larger than the value ($EW \sim 300$ eV) expected from the work of Awaki et al (1991) with $N_{\mathrm{H}} \sim 4 \times 10^{23}$cm^{-2}, taking an opening angle of the torus of about 1/3, as deduced from the optical extended nebula (Pogge 1988). The excess EW could be due to an enhanced iron abundance.

Although the present data cannot provide any meaningful restriction on the depth of any iron K absorption edge at 7.1 keV, and hence on the iron abundance, a deep edge due to a supersolar abundance of iron could partly explain the flat hard X-ray spectra, found in some *Ginga* Seyfert 2

spectra (Awaki et al 1991; Smith & Done 1996), especially when the column density exceeds $N_{\rm H} \sim 10^{23}{\rm cm}^{-2}$.

A similar iron K line feature has been found in *ASCA* spectra of another Seyfert 2 galaxy Mrk 3 (Iwasawa et al 1994). Mrk 3 showed a significant intensity change of the iron K line in response to the continuum variation between two observations of 3.6 yr apart. This fact suggests that the line is produced within ∼1 pc from the central source. We do not of course detect any variability within the present one-day observing run of NGC4388 and therefore cannot obtain any constraint about the line emitting region from this observation.

4.3 The scattered continuum

There is a flat spectral component detected in the intermediate energy range between the hard component and the thermal component. Such a flat component has been observed in *ASCA* spectra of Seyfert 2 galaxies NGC1068 (Ueno et al 1994) and NGC6552 (Fukazawa et al 1994), and the eclipse spectrum of X-ray binary Vela X-1 (Nagase et al 1994). These are considered to be scattered continuum of the central source. It is therefore plausible that this component in NGC4388 is also scattered radiation from the central obscured source, although the possibility that it is radiation from the central source escaping through a partially covering absorber as mentioned in Section 3.1.2. is also viable.

As the broad Hα detected from the off-nuclear region (Shields & Filippenko 1988; 1996) suggests, scattered light may be observed in the optical band. However, spectropolarimetry in the optical blue band does not detect any such broad-line region (Kay 1994).

One can expect that several emission lines produced in the photoionized gas or cold gas which is responsible for the scattering whould be observable on the X-ray continuum, as seen in the *ASCA* spectra of Mrk 3 (Iwasawa et al 1994) and NGC6552 (Fukazawa et al 1994; Reynolds et al 1994). It is, however, hard to detect such lines in our data, because of poorer statistics and contamination by the thermal emission. The detected absorption column density of a few times $10^{22}{\rm cm}^{-2}$ imposed on the power-law is consistent with the narrow-line region reddening E(B–V)∼ 0.5 mag deduced from the [SII] doublet (Malkan 1983), although a recent estimate of the reddening from Paβ/Hβ = 1.1 gives a greater value, E(B–V)∼ 1 mag than this (Ruiz et al 1994). We do however detect a marginally significant iron line due to hydrogenic iron in the SIS spectrum at 6.9 ± 0.1 keV of equivalent width 194 ± 118 eV against the absorbed hard continuum or 4.7 ± 2.9 keV against an extrapolation of the scatttered continuum. The strength of this line is difficult to predict as it is probably due to resonant scattering of the continuum (Matt, Brandt & Fabian 1996), but it does corroborate the scattering hypothesis. To be so highly ionized, the scattering medium is probably within a pc of the nucleus for the observed X-ray luminosity of the central source.

We note that a reasonable fit to the whole SIS spectrum can be obtained with a partially-covered power-law spectrum, with a gaussian line at 6.4 keV and an edge at 0.9 keV. This last feature could be due to a oxygen warm absorber, such as is commonly observed in the spectra of Seyfert 1 galaxies, along the line of sight to the scattering medium. This model is rejected because the *ROSAT* HRI image shows that the scattering medium is much more extended than can be plausibly ionized by the central source (Matt et al 1994).

Other explanations for the flat spectrum are transmission through the edge-on stellar disk, as discussed in the previous section, and a population of high mass X-ray binaries. This last possibility is unlikely given the expected massive star population in the galaxy. The ratio of far infrared luminosity to blue luminosity can be an indicator of relative excess of young population (O stars and high mass X-ray binaries; David et al 1992). Since this ratio in NGC4388, $L_{\rm FIR}/L_{\rm B} = 1.5$, is a factor of 10 lower than in M82, it is unlikely that an intensive starburst like that in M82 is taking place in NGC4388. A collection of X-ray binaries is expected to emit a much smaller X-ray luminosity than that observed ($L_{\rm X} \approx 5 \times 10^{40}{\rm erg\ s}^{-1}$).

4.4 The extended thermal emission

The *ASCA* spectrum, combined with the extended image (Fig. 1) resolved by the *ROSAT* HRI (Matt et al 1994), provides evidence that the soft X-ray emission below 1keV is of thermal origin. Such thermal emission has been observed in the *ASCA* spectra of other nearby spiral galaxies which contain an obscured Seyfert nucleus (e.g., NGC1068, Ueno et al 1994; NGC4258, Makishima et al 1994). The temperature is $kT = 0.47 \pm 0.18$ keV and the abundance is extremely low ($Z = 0.053^{+0.35}_{-0.03} Z_{\odot}$). The 0.5–3 keV luminosity of this thermal emission is $L_{\rm X} = (1.4 \pm 0.3) \times 10^{40}{\rm erg\ s}^{-1}$, consistent with the *Einstein* IPC measurement (Forman et al 1979). Our spectral fits shows most of the observed X-rays below 1.5 keV come from the thermal component (see Fig. 4 and Fig. 5). This is compatible with the fact that most of the X-ray emission detected by the *ROSAT* HRI is extended over the nucleus (Matt et al 1994), taking account for the *ROSAT* bandpass.

The extended thermal gas could be the stripped interstellar medium of the galaxy. Starburst activity is not strong in NGC4388, as discussed in Section 4.3, but consistent with that in normal galaxies with respect to the $L_{\rm X}/L_{\rm FIR}$ correlation (David et al 1992). NGC4388 is known to be located close to the Virgo cluster core, and to move at high velocity of 1311 km s^{-1} relative to the cluster (Corbin et al 1988) in the deep cluster potential The deficiency of HI and CO in this galaxy has been explained in terms of ram-pressure stripping by interaction with the Virgo ICM (Chamaraux et al 1980; Giovanelli & Haynes 1983; Kenney & Young 1986). This stripping mechanism may also explain the X-ray plume of the nearby elliptical galaxy M86 (Forman et al 1979; White et al 1991; Rangarajan et al 1995) which also has similar high radial velocity relative to the cluster (they may be part of an infalling group). The lower temperature and lower abundance in NGC4388 are different from the X-ray plume of M86, however. High quality soft X-ray imaging, such as will be available with *AXAF*, are needed to settle this issue.

Finally, we note that at the radius of the thermal component (1.4–4.5 kpc, Matt et al 1994) the gas density is only ∼ 0.2 cm^{-3}, assuming bremsstrahlung emission since the abundance is so low, and any scattered X-ray emission will be negligible. The bremsstrahlung emission from any scattering medium at a temperature $> 10^6$ K would swamp

the scattered flux. The radiative cooling time of the gas is $\sim 10^8$ yr and the recombination time (of say highly ionized oxygen) is $< 10^6$ yr. The flow time at a velocity of 300 km s^{-1} is $\sim 10^7$ yr. The gas may therefore be due to an outburst in the last ten million yr, or a more general wind from the nuclear regions. The mass flow rate is then about $\dot{M}\sim 100 v_{300} R_2^2 M_\odot \mathrm{yr}^{-1}$ where v_{300} is a wind velocity in unit of 300 km s^{-1} and R_2 is the radius of the thermal emission region in units of 2 kpc, which is at the highest end of the values for superwind galaxies ($\dot{M}\sim$1–100$M_\odot$yr^{-1}, Heckman, Armus & Miley 1991). This large mass injection is unlikely for NGC4388 since it shows no evidence for a strong starburst such as in superwind galaxies. The low measured abundance (though error is rather large) is also puzzling. It is however measured mainly for iron-L in our spectrum. As the abundance of iron is usually lower than that of other elements in starburst galaxies, the low abundance may not be unusual if the thermal emission is produced through a recent starburst.

4.5 A consistent solution for NGC4388

We have identified several problems in the interpretation of the X-ray data of NGC4388: a) the large soft X-ray extent, if thermal, means a large mass loss rate from the bulge which can only plausibly last a few million yr, b) a thermal model requires a very low abundance in the extended gas and c) the iron line is high for the observed obscuration (and in the case of an iron line from reflection assuming that the solid angle subtended by this and thicker gas at the nucleus is from a toroidal geometry aligned with the disk of the galaxy).

These unusual propoerties can be solved if we assume that the nucleus has not always had its present luminosity, $L_{\rm x}$, but had a higher luminosity, $L'_{\rm x}$ a thousand years or more ago when gas at the radius of the soft X-ray extent ($\sim$ 1.5 kpc) was being irradiated. The warm absorber solution in Section 4.3 requires that the ionization parameter, $\xi = L/nR^2$ where the density of gas at radius R is N, is ~ 100. Then

$$L'_{\rm x} = \xi n R^2 = \xi \frac{L_s}{f\sigma L'_{\rm x}} R,$$

where f is the fraction of the volume within R being irradiated and σ is the Thomson cross-section. We then find $L'_{\rm x} \sim f^{-1/2} 10^{44}$erg s^{-1}, the Thomson depth of the region is then $\sim f^{-1/2} 2\times 10^{-4}$ and the density $\sim f^{-1/2} 0.06$ cm^{-3}. Provided that f is not small the luminosity is plausible for a central engine of more than $10^6 M_\odot$. It is possible that the optical line emission only shows up one side of a very wide cone so $f > 0.5$.

With this solution, all of the X-ray emission below 3 keV can be due to scattering by partially-ionized gas within a few kpc of the nucleus. The feature in the spectrum around 1 keV is then due to absorption by OVIII. The OVIII absorption edge would be produced in a region close to the nucleus as found in MCG–6-30-15 (Otani et al 1996). The presence of dust in the ionized gas implied from the optical/near infrared extinction is not peculiar but similar to the dusty warm absorber observed in IRAS13349+2438 (Brandt, Fabian & Pounds 1996) as well as MCG–6-30-15. The nucleus must have been 100 or more times more luminous in the past. Enhanced iron K-line emission could be produced by gas in the bulge and disk of the galaxy (see Fabian 1977).

A continuous decrease in X-ray luminosity over a long time scale has been observed in some Seyfert galaxies such as NGC 2992 (Weaver et al 1996), Mrk 3 (Iwasawa et al 1994) and NGC 1275 (A. Edge, private communication). The Seyfert 1.9 galaxy NGC2992, for example, has declined in luminosity by more than a factor of 20 over the last 17 yr. The luminosity variation is similar to that found for those Seyfert galaxies, except that in NGC4388 we require a larger variation over a longer timescale. As discussed for Mrk 3 (Iwasawa et al 1994) and NGC 2992 (Weaver et al 1996), a reverberation effect makes the EW of the iron K line large if the X-ray luminosity decreases continuously.

The main problem is the lack of observed optical polarization. This could however be low due to the small extraction window used by Kay (1994), which mainly sampled the region obscured by the galaxy disk, and to a wide opening angle for the emerging radiation, which reduces the predicted level of polarization. Further spectropolarimetric observations of a wider region are required.

5 SUMMARY

We find from the *ASCA* observations that the spectrum of the Seyfert 2 galaxy NGC4388 has many components. The hard X-ray emission is strongly absorbed, and a strong iron K line ($EW \approx$ 440–730 eV) is found at 6.4 keV. The hard continuum has a photon index $\Gamma \approx 1.6$ and is absorbed by a column density $N_{\rm H} \approx 4\times 10^{23}$cm^{-2}. Evidence for a thermal spectrum is found in the soft X-ray band, which can be identified with the spatially extended emission observed by *ROSAT* HRI (Matt et al 1994). A flat spectrum joins these two components in the band around 2 keV. It may be the scattered continuum of the obscured central source. However, several difficulties still remain; (1) an extremely low abundance is required for the thermal emission model; (2) an unlikely high mass flow rate is required to explain the soft X-ray extent; and (3) the iron-K line stronger than expected from the torus model, with the observed column density. These can be overcome if the central source was a hundred times brighter a thousand or more years ago. All the soft X-ray emission below 3 keV can then be due to the continuum scattered in a partially ionized medium irradiated by the luminous source. The iron K line produced by gas in the bulge and disk in the galaxy then remains strong, because of the larger size. This will be tested by a detailed imaging spectroscopy with future missions like *AXAF* and *Astro-E*.

ACKNOWLEDGEMENTS

We thank all the members of the *ASCA* PV team, Giorgio Matt and David White for useful discussion and Niel Brandt for helping to make the *ROSAT* HRI image. The optical image of NGC4388 was obtained through the *Sky View* facility operated by HEASARC at NASA/GSFC. This research has made use of data obtained through the High Energy Astrophysics Science Archive Research Center Online Service, provided by the NASA-Goddard Space Flight Center. ACF

and KI thank the Royal Society and PPARC, respectively for support.

REFERENCES

Antonucci R.R.J., 1993, ARAA, 31, 473
Antonucci R.R.J., Miller J.S., 1985, ApJ, 297, 621
Awaki H., et al, 1994, PASJ, 46, L65
Awaki H., Koyama K., Inoue H., Halpern J.P., 1991, PASJ, 43, 195
Böhringer H., Briel U.G., Schwarz R.A., Voges W., Hartner G., Trümper J., 1994, Nat, 368, 828
Brandt W.N., Fabian A.C., Pounds K.A., 1996, MNRAS, 278, 326
Chamaraux P., Balkowski C., Gerald E., 1980, A&A, 83, 5
Colina L., 1992, ApJ, 386, 59
Colina L., Fricke K.J., Kolatschny W., Perryman M.A.C., 1987, A& A, 186, 39
Corbin M.R., Baldwin J.A., Wilson A.S., 1988, ApJ, 334, 584
David L.P., Forman C., Jones W., 1992 ApJ, 388, 82
Fabian A.C., 1977, Nat, 269, 672
Filippenko A.V., Sargent W.L.W., 1985, ApJS, 57, 503
Forman W., Schwartz J., Jones D., Liller W., Fabian A.C., 1979, ApJ, 234, L27
Fukazawa Y. et al 1994, PASJ, 46, L141
Giovanelli R., Haynes M.P., 1983, AJ, 88, 881
Ghisellini G., Haardt F., Matt G., 1994, MNRAS, 267, 743
Hanson C.G., Skinner G.K., Eyles C.J., Wilmore A.P., 1990, MNRAS, 242, 262
Heckman T.M., Armus L., Miley G.K., 1991, ApJS, 74, 833
Hummel E., Saikia D.J., 1991, A&A, 249, 43
Iwasawa K., Yaqoob T., Awaki H., Ogasaka Y., 1994, PASJ, 46, L167
Iwasawa K., Koyama K., Awaki H., Kunieda H., Makishima K., Tsuru T., Ohashi T., Nakai N., 1993, ApJ, 409, 155
Kay L.E., 1994, ApJ, 430, 196
Kenney J.D., Young J.S., 1986, ApJ, 301, L13
Koyama K., Takano S., Tawara Y., 1991, Nat, 339, 603
Krolik J.H., Madau P., Życki P.T., 1994, ApJ, 420 L57
Lebrun F., et al 1992, A&A, 264, 22
Makishima K., Fujimoto R., Ishisaki Y., Kii T., Loewenstein R. Mushotzky R., Serlemitsos P., Sonobe T., Tashiro M., Yaqoob Y., 1994, PASJ, 46, L77
Malkan M.A., 1983, ApJ, 264, L1
Matsushita K. et al, 1994, ApJ, 436, L41
Matt G., Piro L., Antonelli L.A., Fink H.H., Meurs E.J.A., Perola G.C., 1994, A&A, 292, L13
Matt G., Brandt W.N., Fabian A.C., 1996, MNRAS, 280, 823
McLeod K.K., Rieke G.H., ApJ, 441, 96
Nagase F., Zylstra G., Sonobe T., Kotani T., Inoue H., Woo J., 1994, ApJ, 436, L1
Otani C., et al 1996, PASJ, 48, 211
Phillips M.M., Malin D.F., 1982, MNRAS, 199, 905
Phillips M.M., Charles P.A., Baldwin J.A., 1983, ApJ, 266, 485
Pogge R.W., 1988, ApJ, 332, 702
Rangarajan F.V.N., White D.A., Ebeling H., Fabian A.C., 1995, MNRAS, 277, 1047
Reynolds C.S., Fabian A.C., Makishima K., Fukazawa Y., Tamura T., 1994, MNRAS, L55
Ruiz M., Rieke G.H., Schmidt G.D., 1994, ApJ, 423, 608
Rush B, Malkan M.A, 1996, AJ, in press
Sandage A., Tammann G.A., 1984, Nat, 307, 326
Shields J.C., Filippenko A.V., 1988, ApJ, 332, L55
Shields J.C., Filippenko A.V., 1996, A&A, 311, 393 (RN)
Smith D.A., Done C., 1996, MNRAS, 280, 355
Stone J.L., Wilson A.S., Ward M.J., 1988, ApJ, 330, 105
Tadhunter C., Tsvetanov Z., 1989, Nat, 341, 422
Takano S., Koyama K., 1991, PASJ, 43, 1
Ueno S., Mushotzky R.F., Koyama K., Iwasawa K., Awaki H., Hayashi I., 1994, PASJ, 46, L71
Weaver K.A., Nousek J., Yaqoob T., Mushotzky R.F., Makino F., Otani C., 1996, ApJ, 458, 160
White D.A., Fabian A.C., Forman W., Jones C., Stern C., 1991, ApJ, 375, 35
Wilson A.S., Elvis M., Lawrence A., Bland-Hawthorn J. 1992, ApJ, 391, L75
Yaqoob T., 1996, ApJ, in press